

The Bjerknes feedback in the tropical Atlantic in CMIP5 models

Anna-Lena Deppenmeier^{1,2}  · Reindert J. Haarsma² · Wilco Hazeleger^{1,2,3}

Received: 1 April 2015 / Accepted: 14 January 2016 / Published online: 10 February 2016
© The Author(s) 2016. This article is published with open access at Springerlink.com

Abstract Coupled state-of-the-art general circulation models still perform relatively poorly in simulating tropical Atlantic (TA) climate. To investigate whether lack of air-sea interaction might be responsible for their biases, we investigate the Bjerknes feedback (BF) in the TA, the driver of the dominant interannual variability in that region. First, we analyse this mechanism from reanalysis data. Then, we compare our findings to model output from the Coupled Model Intercomparison Project Phase 5. The feedback is subdivided into three components. The first one consists of the influence of eastern equatorial sea surface temperature anomalies (SST') on zonal wind stress anomalies (τ_u') in the western basin. The second component is the influence of wind stress anomalies in the western TA on eastern equatorial oceanic heat content anomalies (HC'). The third component is the local response of overlying SST' to HC' in the eastern TA. All three components are shown to be present in ERA-Interim and ORAS4 reanalysis by correlating the two variables of each component with each other. The obtained patterns are compared to the ones from model output via pattern correlation per component. While the models display errors in the annual cycles of SST, τ_u , and HC, as well as in the seasonality of the feedback, the impact of SST' on wind stress and the impact of wind stress on HC' are simulated relatively well by most of the models. This is especially the case when correcting

for the error in seasonality. The third component of the BF, the impact of HC' on SST' in the eastern part of the basin, deviates from what we find in reanalysis. We find an influence of HC anomalies on overlying SSTs in the eastern equatorial TA, but it is weaker than in the reanalysis and it is not strongly confined to the equator. Longitude-depth cross sections of equatorial temperature variance and correlation between subsurface temperature anomalies and SST' in the cold tongue region show that flawed simulation and slow adjustment of the subsurface ocean are responsible for this.

Keywords Tropical Atlantic variability · Bjerknes feedback · Air-sea interaction · Climate modeling

1 Introduction

In spite of an overall performance improvement in simulating the world's climate, coupled general circulation models (CGCMs) still display large biases in the tropical Atlantic (TA), both in the ocean and in the atmospheric circulation. Most CGCMs are unable to reproduce the observed cold tongue in the eastern part of the TA basin and there are biases in the slope of the equatorial thermocline (Richter and Xie 2008; Davey et al. 2002; Chang et al. 2007). Furthermore, there are biases in simulating tropical Atlantic variability (TAV).

A prerequisite of simulating TA climate correctly is that the mechanisms that govern TA climate and its variability are well represented in the models. While the large annual cycle causes most of the SST variability in the TA, two other leading modes of interannual to decadal variability have been identified: the zonal and the meridional mode. The zonal mode with a period of two to four years is driven by the Bjerknes feedback (in the following abbreviated as BF) (Ruiz-Barradas et al. 2000; Keenlyside and Latif 2007; Janssen et al. 2008), whereas the

✉ Anna-Lena Deppenmeier
anna-lena.deppenmeier@wur.nl

¹ Meteorology and Air Quality Department, Wageningen University, Post Box 47, 6700 AA Wageningen, The Netherlands

² R&D Weather and Climate Modeling, Royal Netherlands Meteorological Institute (KNMI), Utrechtseweg 297, 3731 GA, De Bilt, The Netherlands

³ Netherlands eScience Center (NLeSC), Science Park 140, 1098 XG Amsterdam, The Netherlands

meridional mode on decadal time scales (Zebiak 1993; Carton et al. 1996; Xie and Carton 2004, e. g.) arises through the wind evaporation sea surface temperature (WES) feedback (Chang et al. 1997). In this paper we will focus on the zonal mode.

Previous studies have identified the BF as driving mechanism of the zonal mode in reanalysis data. Keenlyside and Latif (2007) found the BF to be present in the TA. Janssen et al. (2008) found not only the BF, but also the recharge oscillator to be a dominant driver of TAV. Ding et al. (2010) confirmed the presence of the BF with principal oscillation pattern analysis, and investigated the seasonality of the upper equatorial Atlantic (Ding et al. 2009). A connection between the two modes of variability has been suggested by Foltz and McPhaden (2010), and a connection between the zonal mode and the Benguela Niño has been suggested by Lübecke et al. (2010). Several studies have investigated the feedbacks in the TA with the help of general circulation models (GCMs) (DeWitt 2005; Mahajan et al. 2009; Muñoz et al. 2012; Ding et al. 2015).

Most state-of-the-art CGCMs simulate the mean state and variability in the TA poorly (Breugem et al. 2006). This has often been attributed to the westerly wind bias along the equator (Richter and Xie 2008). Hazeleger and Haarsma (2005) show that vertical mixing can play an important role and (Li and Xie 2012) propose that tropical-wide SST errors arise from incorrect simulation of cloud cover and thermocline depth. A recent study by Ding et al. (2015) shows that an improved mean state of the TA can lead to better representation of interannual variability. Our study aims to quantify the strength and phase of the air-sea interaction related to the BF in newest generation climate models, and possibly point to weaknesses in the model representation. We do so by considering different aspects of the feedback and perform statistical analysis on reanalysis and model data. Below, we shortly outline the BF.

In the warm phase of the zonal mode, positive sea surface temperature anomalies (SST') in the eastern part of the basin cause the zonal winds (τ_u) in the western part of the TA to weaken. The associated weakening of the zonal pressure gradient allows the thermocline in the eastern basin to deepen and thereby increases the oceanic heat content (HC) in the region. This reduces entrainment of colder subsurface waters into the turbulently mixed surface layer. In addition, the weaker winds may lead to less atmospheric cooling by turbulent surface heat fluxes. The result is a strengthening of the positive SST' in the region, closing the feedback loop. The opposite happens in the cold phase of the zonal mode (Zebiak 1993).

As a reference for the model results we use a set of reanalysis data which has, to our knowledge, not yet been used for the analysis of the zonal mode. We consider monthly as opposed to seasonal time series because of the pronounced annual cycle in the region. It has been suggested that the zonal mode can be understood as an interannual variation

of the strength of the cold tongue (Burls et al. 2011, 2012). This leads to the hypothesis that if the annual cycle is simulated incorrectly, either in timing or strength, the representation and mechanism of the zonal mode will be flawed as well. Therefore, we compare the simulated annual cycles to annual cycles in the reanalysis before analysing the BF components. This allows us to a posteriori correct the model output for the errors in their annual cycles and to assess whether the mechanism driving the zonal mode is correctly represented in other months than in the reanalysis. Finally, we analyse the simulated subsurface ocean and its interaction with SST' as compared to reanalysis.

This paper is structured as follows: in Sect. 2 we describe the data and methodology, in Sect. 3 we investigate the BF in reanalysis data, and in Sect. 4 we compare first the annual cycle (Sect. 4.1), and subsequently the three components of the BF (Sects. 4.2, 4.3) to reanalysis data. In Sect. 4.4 we examine subsurface temperature variance and its correlation to SST' in the TA, followed by the conclusions of this study in Sect. 5.

2 Data and methodology

The reanalysis data used in this study is obtained from the European Centre for Medium-Range Weather Forecasts (ECMWF). The variables τ_u and SST are taken from the global atmospheric reanalysis ERA-Interim (Dee et al. 2011), and the potential ocean temperature from the Ocean Reanalysis System 4 (ORAS4) (Balmaseda et al. 2013). Note that the SST from ERA-Interim and ORAS4 do not differ significantly, since ERA-Interim was used to drive the ocean reanalysis for 20 years out of the 35 years we use in this study. We use time series from 1979 until 2013, due to availability (ERA-Interim) and trustworthiness of the data (ORAS4). For the first years of ORAS4, 1958 until 1979, before the satellite era, little data is available to constrain the reanalysis.

The model output used in this study is obtained from the Coupled Model Intercomparison Project Phase 5 (CMIP5) (Taylor et al. 2012). The CGCMs as well as the markers indicating them in the comparison plots, and the centers where the simulations were performed are shown in Table 1. We use the last 150 years of the pre-industrial control runs to investigate the natural variability in absence of anthropogenic forcing and with minimised model drift. It is noteworthy that the warm SST bias in those simulations is as large as it is. We are comparing the CGCM output to current reanalysis data which already includes the global warming in response to the heightened CO₂ forcing. The CGCM output we use was produced with pre-industrial forcing and should therefore be colder than the reanalysis data.

Table 1 Models used in this study, the markers denoting them in the graphics, and the centers where the simulations were run. For more information we refer to CMIP5 (2015)

Number	Marker	Model	Center	Number	Marker	Model	Center
1	◆	ACCESS1-0	CSIRO-BOM	19	◆	GFDL-ESM2M	NOAA GFDL
2	◇	ACCESS1-3	CSIRO-BOM	20	◀	GISS-E2-H	NASA GISS
3	●	bcc-csm1-1	BCC	21	◀	GISS-E2-H-CC	NASA GISS
4	●	bcc-csm1-1-m	BCC	22	◀	GISS-E2-R	NASA GISS
5	▲	CanESM2	CCCma	23	◀	GISS-E2-R-CC	NASA GISS
6	●	CCSM4	NCAR	24	●	HadGEM2-CC	MOHC
7	◊	CESM1-BGC	NSF-DOE-NCAR	25	●	HadGEM2-ES	MOHC-INPE
8	◊	CESM1-CAM5	NSF-DOE-NCAR	26	○	IPSL-CM5A-LR	IPSL
9	◊	CESM1-CAM5-1-FV2	NSF-DOE-NCAR	27	●	IPSL-CM5A-MR	IPSL
10	◊	CESM1-FASTCHEM	NSF-DOE-NCAR	28	●	IPSL-CM5B-LR	IPSL
11	◊	CESM1-WACCM	NSF-DOE-NCAR	29	●	MIROC-ESM	MIROC
12	■	CMCC-CESM	CMCC	30	●	MIROC-ESM-CHEM	MIROC
13	■	CMCC-CM	CMCC	31	◀	MPI-ESM-LR	MPI-M
14	■	CMCC-CMS	CMCC	32	◀	MPI-ESM-MR	MPI-M
15	+	CNRM-CM5	CNRM-CERFACS	33	◀	MPI-ESM-P	MPI-M
16	↖	CSIRO-Mk3-6-0	CSIRO-QCCCE	34	▲	MRI-CGCM3	MRI
17	✗	FIO-ESM	FIO	35	◇	NorESM1-M	NCC
18	◊	GFDL-CM3	NOAA GFDL	36	◆	NorESM1-ME	NCC

All data are interpolated to a $1^\circ \times 1^\circ$ grid and linearly detrended using monthly mean time series.

The upper ocean heat content is calculated grid-pointwise by integrating the potential ocean temperature upwards from the 293.15 K isotherm depth to the surface according to Eq. 1.

$$HC(lat, lon) = c_p \cdot \rho \int_{Z_{20}}^0 T(z, lat, lon) dz, \quad (1)$$

where we assume a uniform density ρ of 1024.75 $\frac{kg}{m^3}$ and a specific heat capacity c_p of 3993 $\frac{J}{kg \cdot K}$ for sea water (Laboratory 2015).

We use the following index regions as indicators for the western TA (WA4, 4°N — 4°S ; 40°W — 20°W) and the eastern TA (EA4, 4°N — 4°S and 20°W — 10°E), cf. Fig. 2. The variables and correlations are spatially averaged over these index regions to obtain a time series or a mean value. Note that for the sample size used (length of the time series) and degrees of freedom of the data, the threshold value for a

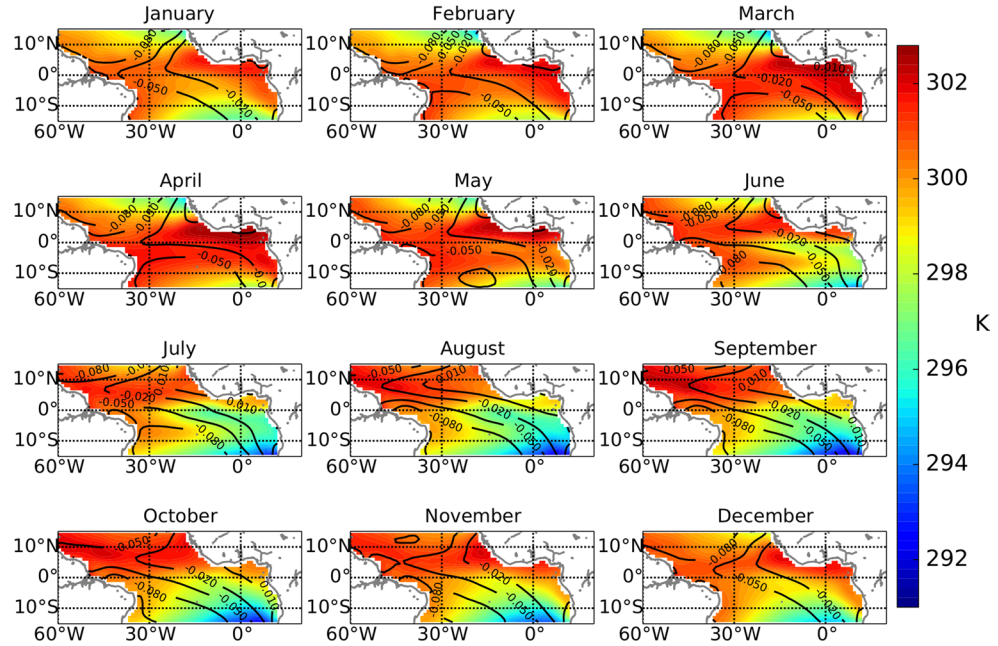
95 % significant correlation is 0.35. The signal can be considered significant when the number of gridpoint correlations exceeding that threshold is larger than 5 %. Note that the variance that is explained by a correlation of 0.35 is still relatively small.

3 Bjerknes feedback in reanalysis data

In this section we investigate characteristics of the zonal mode in the TA from reanalysis data. Because of the close connection of the zonal mode to the annual cycle mentioned above, we first examine the annual cycles of SST, τ_u , and HC, and subsequently the correlations between the variables.

The strong annual cycle of SST in the basin is evident from Fig. 1. During boreal winter direct solar radiation warms the ocean with high intensity, temperatures peak in boreal spring when they reach values larger than 300 K (27°C). From May onward the temperature distribution

Fig. 1 Climatology obtained from ERAInterim reanalysis of SST [K] and τ_u [$\frac{N}{m^2}$] in the TA throughout the year



changes: the warm waters retreat north-westwards from the east and a cold tongue forms during boreal summer, spanning the region around the equator and covering the whole eastern to central part of the basin. This cooling is thought to be caused by upwelling of cold water in the eastern part of the basin, which is closely linked to the sudden onset of the West African Monsoon (Mitchell and Wallace 1992). With strengthening of the westward winds and cooling of the SST the BF becomes active (Burls et al. 2011). The cold tongue is most prominent in August. From September onward, upwelling is reduced through weakening of the southerly cross-equatorial winds, and the cold tongue retreats.

The cold tongue region displays high SST variability on both annual and interannual time scales. Correlating monthly SST time series of the chosen cold tongue index EA4 to the monthly time series of SST over the whole basin yields the pattern of the interannual mode of SST variability, the zonal mode. Performing regression analysis in the same manner delivers information about the strength of this mode of variability. Both are shown in Fig. 2.

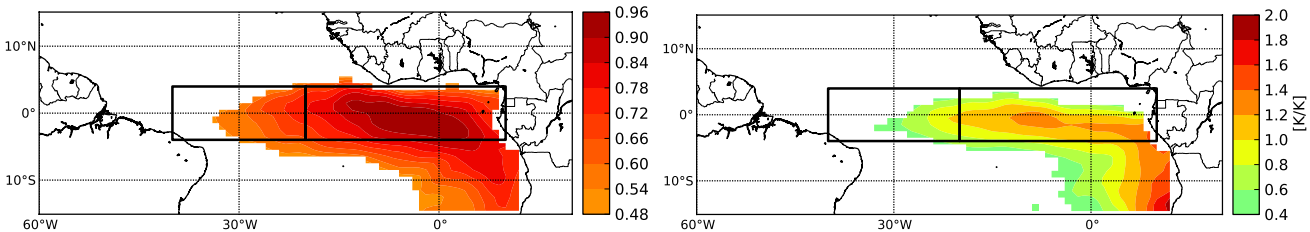


Fig. 2 The zonal mode obtained from ERA-Interim averaged over June, July and August. *Left* correlation between monthly SST in EA4 (right box), and SST elsewhere in the basin. The *left box* indicates the

The BF consists of three components: the influence of SST anomalies in the eastern part of the equatorial Atlantic basin on τ_u ($\lambda_{SST \rightarrow \tau_u}$), the effect of τ_u anomalies in the west on the east-equatorial HC ($\lambda_{\tau_u \rightarrow HC}$), and the local effect of the HC anomalies on overlying SSTs ($\lambda_{HC \rightarrow SST}$) in the cold tongue region. The connection between the two variables of the three components can be illustrated by correlating the anomaly time series to another according to Eq. 2, where σ_a and σ_b are the standard deviations of variable a and b , respectively, and primes denotes anomalies.

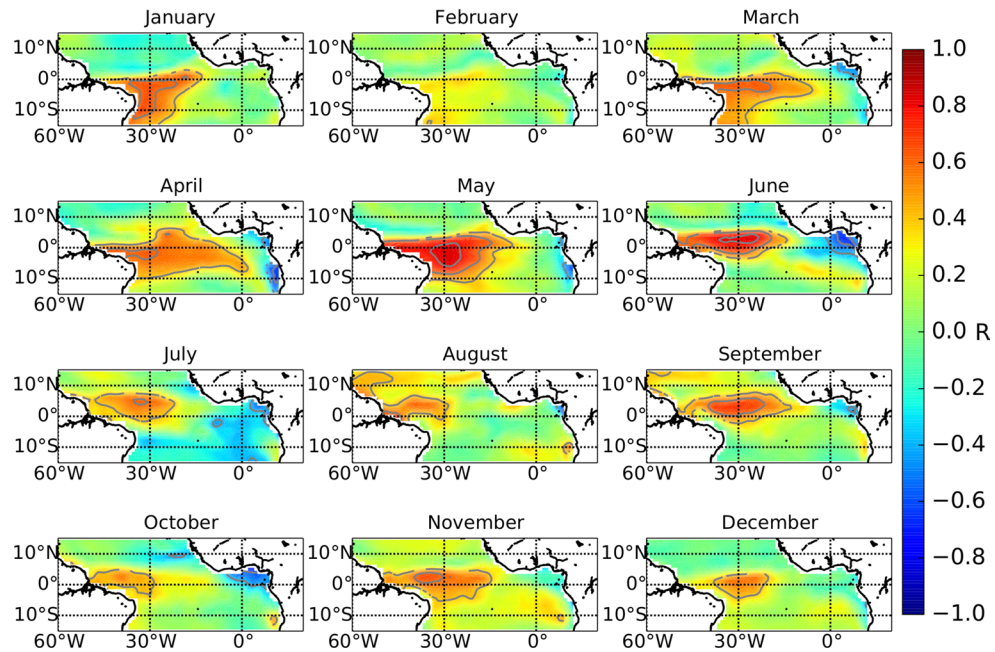
$$r(lat, lon) = \frac{\sum a'(t) \cdot b'(t, lat, lon)}{\sigma_a \cdot \sigma_b} \quad (2)$$

Appropriate indices are chosen to represent the eastern and the western basin (see Fig. 2 and Sect. 2) for variable a .

In order to detect the separate components of the BF, we adapt a method similar to Keenlyside and Latif (2007). For each component of the feedback we correlate the spatially averaged timeseries of anomalies in the region of interest of variable a point-wise to the time series of variable b . Each

WA4 index used for other correlation analysis later on. *Right* linear regression analysis of monthly SST'EA4 on monthly SST' elsewhere

Fig. 3 Correlation pattern obtained from reanalysis (ERA-Interim) between SST anomaly in EA4 and wind stress anomalies for each month of the year, the first component of the BF $\lambda_{SST \rightarrow \tau_u}$. Contours indicate significant correlation at the 90 % confidence level



of the interactions is investigated separately for every calendar month.

For the first component of the BF, $\lambda_{SST \rightarrow \tau_u}$, we average SST' over the box EA4 (see Fig. 2). The box was chosen to be slightly larger than reported in previous literature in order to avoid constraining the model output too much. In Fig. 3 the correlations between SST' and τ_u' are shown for each month of the year. Because the response time of the atmosphere to SST' is less than a month, we use a zero month lag for $\lambda_{SST \rightarrow \tau_u}$.

A significant correlation associated with the first component of the BF appears in March, broadens in April, and is strongest in the western Atlantic along the equator in May. The equatorial response of τ_u to SST' extends to a large area north and south of the equator. In June the area of highest correlation departs from the equator, indicating that another mechanism, possibly connected to the migrating ITCZ becomes more important. In July, the area with maximum correlations has moved northward together with the ITCZ.

The second component of the BF, $\lambda_{\tau_u \rightarrow HC}$, describes the impact of wind stress anomalies in the western part of the basin on the eastern equatorial oceanic HC. τ_u' in the west generate Kelvin waves that propagate eastward along the equatorial waveguide and cause a deepening of the thermocline in the east, thereby increasing the upper ocean HC. Due to the time it takes a Kelvin wave to travel from east to west we introduce a lag of 1 month when correlating the two variables in order to exclude direct influences of τ_u on HC via an atmospheric pathway. To identify $\lambda_{\tau_u \rightarrow HC}$, we average τ_u over the box WA4 (see Fig. 2) and correlate the anomalies to the HC' in a point-wise manner. While testing

the sensitivity of the results to the chosen lag, we observe that the highest correlation between τ_u' and HC' with a BF like pattern occurs at zero month lag in the reanalysis data, although the results are very similar to a 1 month lag. We hypothesise that other mechanisms than the BF, such as Ekman pumping, can be responsible for this, and therefore retain the 1 month lag.

The monthly results are shown in Fig. 4. We notice a build up of high correlation centered on the equator in March–April and a further increase in April–May. The correlation weakens in May–June, and fades into a pattern that is reminiscent of a discharge process in June–July. The timing of the correlation and its maximum strength in May coincides with that of $\lambda_{SST \rightarrow \tau_u}$, suggesting that the two processes are closely connected. In July, the pattern clearly deviates from the expected $\lambda_{\tau_u \rightarrow HC}$ pattern associated with the BF. This is also the case for $\lambda_{SST \rightarrow \tau_u}$, and indicates the end of the season when the BF is active.

The third component of the BF describes the influence of oceanic HC on overlying SST', $\lambda_{HC \rightarrow SST}$; mainly to be seen in the cold tongue region where the thermocline is shallow and allows cold subsurface waters to mix with the warm surface waters (Fig. 5). This is the least well-defined of the three components, displaying correlations between subsurface anomalies and SST' in several regions of the basin. Focusing on the equator, the correlation increases as early as April, albeit very weakly at this stage. The signal peaks in May, and persists throughout June. In the latter month, the signal is still located almost symmetrically along the equator, which is hardly the case for $\lambda_{SST \rightarrow \tau_u}$. The signal quickly vanishes afterward, consistent with the timing of the other two components which have also begun to

Fig. 4 Correlation pattern obtained from reanalysis (ERA-Interim) between τ_u anomaly (ERA-Interim) in WA4 and upper ocean HC anomalies (derived from ORAS4) elsewhere in the basin for each month of the year, the second component of the BF $\lambda_{\tau_u \rightarrow HC}$. Contours indicate significant correlation at the 90 % confidence level

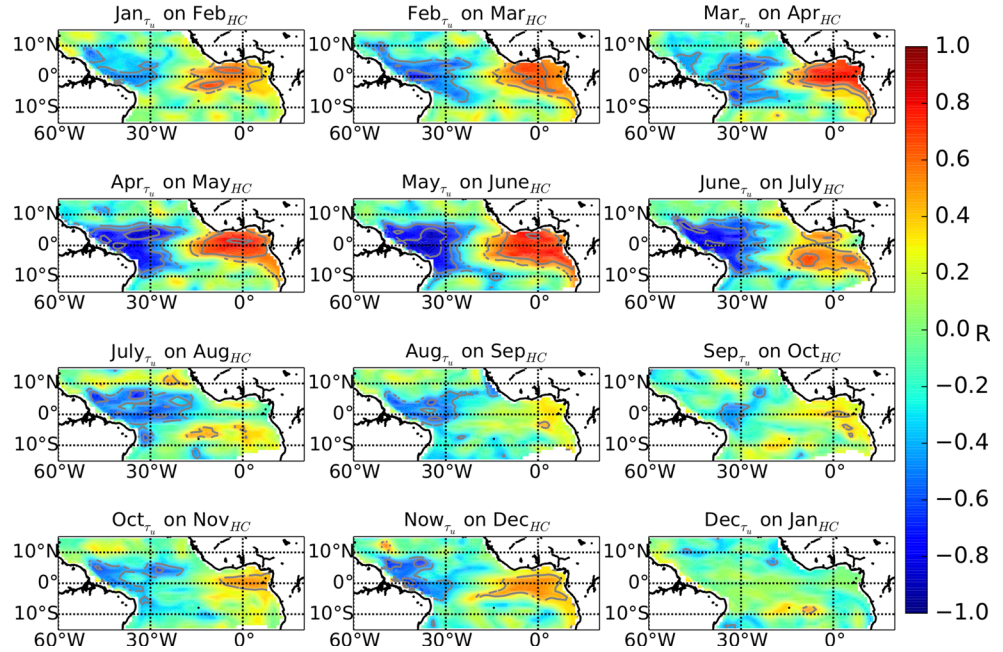
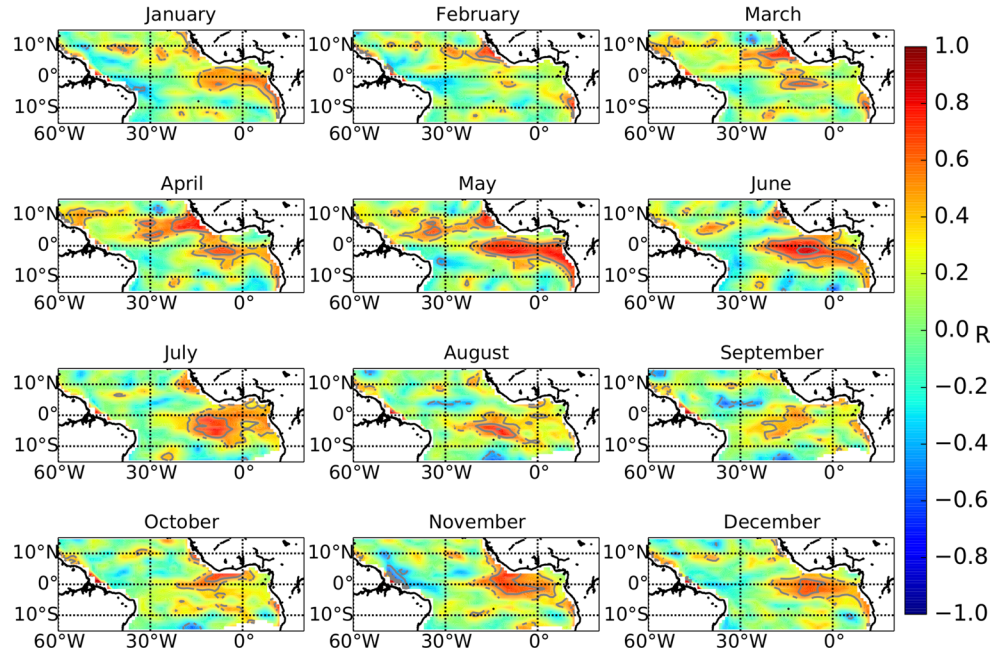


Fig. 5 Correlation pattern obtained from reanalysis between upper ocean HC anomalies (derived from ORAS4) and SST anomalies (ERA-Interim), correlated pointwise, component three of the BF $\lambda_{HC \rightarrow SST}$. Contours indicate significant correlation at the 90 % confidence level



cease by that time. There is also a significant correlation signal in November up to January, indicative of the second peak of the zonal mode described by Okumura and Xie (2006). Signs of this can also be found in the other two components of the BF loop shown above.

From the monthly stratified correlation analysis of reanalysis data we conclude that the BF mechanism indeed exists in the TA, confirming earlier studies. The activity of the three components coincides in May and June, when distinct correlation patterns are visible. Zonal wind stress anomalies originate from SST' early in the year (March,

April). In these months, τ_u' induce oceanic perturbations in the western part of the TA that travel to the east of the basin. There, the ocean stratification reaches a state in May in which the $\lambda_{HC \rightarrow SST}$ coupling is possible. The resulting SST' again affect the atmospheric circulation along the equator, impacting τ_u' . During these months the feedback loop is active. The equatorial atmospheric response decreases in June, when the atmosphere is influenced by other factors, most importantly the migration of the ITCZ. Remnants of the feedback loop can be observed in July, although other mechanisms seem to more dominant at this point.

In contrast to other studies about the BF, we show a monthly stratified picture of the BF. It becomes clear that the signal is not always centered on the equator throughout boreal summer. Other processes seem to mix with the BF leading to correlation patterns that deviate from the one found by Keenlyside and Latif (2007). Their study also analyses the seasonality of the BF. Our results are in line with the authors' finding that $\lambda_{SST \rightarrow \tau_u}$ is mostly active in boreal spring and early boreal summer, and that $\lambda_{HC \rightarrow SST}$ is mostly active in late boreal spring and early summer. The regression analysis in Keenlyside and Latif (2007) indicates a coupling until as late as August, which we cannot confirm, as the signal is no longer centered on the equator in our analysis. While the tropical Atlantic atmosphere is still sensitive to SST' in the east, the BF loop is not completed by an equatorial Kelvin wave. In the reanalysis data set analysed here the oceanic response of HC to τ_u' is also subject to seasonal modulation. The signal on the equator is most prominent in boreal spring until early boreal summer.

We have demonstrated that it is important to look at the monthly stratified picture of the tropical Atlantic when investigating the BF, as the correlation patterns of the three components vary strongly between the months. We continue to examine the CGCMs performance in the months May, June, and July. During May and June the correlation patterns are most distinct, especially for $\lambda_{SST \rightarrow \tau_u}$ and $\lambda_{HC \rightarrow SST}$. In July the correlation strength weakens and the pattern changes, indicating the end of the BF.

4 Comparison between reanalysis and model output

4.1 Annual cycle

In the former section we have established that a BF exists in the equatorial Atlantic ocean, confirming other studies (Keenlyside and Latif 2007; Okumura and Xie 2006). It is strongest in the early boreal summer months May and

June and fades in July. In the following we will compare the model output to reanalysis data in order to investigate whether the models capture the BF. Because of the strong seasonality and the phaselocking to the annual cycle we will first compare the annual cycle of the reanalysis to those of the models, as shown in Fig. 6. The three variables that are related to the BF, SST, τ_u , and HC, are examined in the regions of interest for the BF, i. e., EA4 for SST and HC, and WA4 for τ_u .

In all three panels of Fig. 6 there are obvious deviations of the model output from reanalysis, and there is a large spread between the models. For SST (left panel of Fig. 6) the models simulate the annual cycle reasonably well during boreal winter and early spring. The model ensemble mean almost coincides with reanalysis from November to April. This implies an overall warm bias in the CGCMs, as pre-industrial control simulations are used. From May onward the reanalysis SST cools strongly, generating a slope that none of the models reproduces. In the following months the models' SST lag behind reanalysis SST, reaching their minimum SST one to 2 months later than in the reanalysis data. Another feature in the CGCMs' SST annual cycle is their relatively weak amplitude, especially during boreal summer and fall. The weak cooling of eastern equatorial SST is associated with the models' inability to reproduce the boreal summer cold tongue.

The annual cycle of τ_u in the western part of the basin displays similar shortcomings (center panel of Fig. 6). Overall, τ_u is markedly underestimated by almost all CGCMs under investigation. None of the examined CMIP5 models simulate the weakening of the winds in September and the following strengthening in November associated with the second zonal mode (second Niño, Okumura and Xie 2006). In the reanalysis τ_u reaches its minimum in April, while several models simulate τ_u at its weakest in May, some even in June. τ_u in the reanalysis reaches its first local maximum in August, while most of the models simulate strengthening until September. This is in agreement with the lag we also find for the minimum of τ_u , but is also

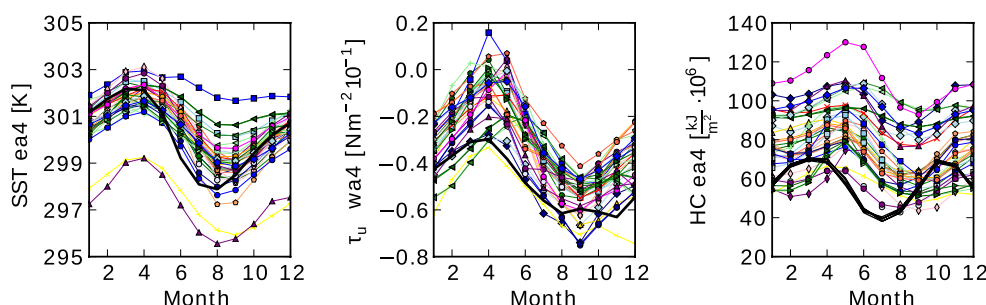


Fig. 6 Seasonal cycles of the variables relevant to the BF: SST in EA4, τ_u in WA4, and upper ocean HC in EA4. Reanalysis data is plotted in black, for reference of the individual models see Table 1

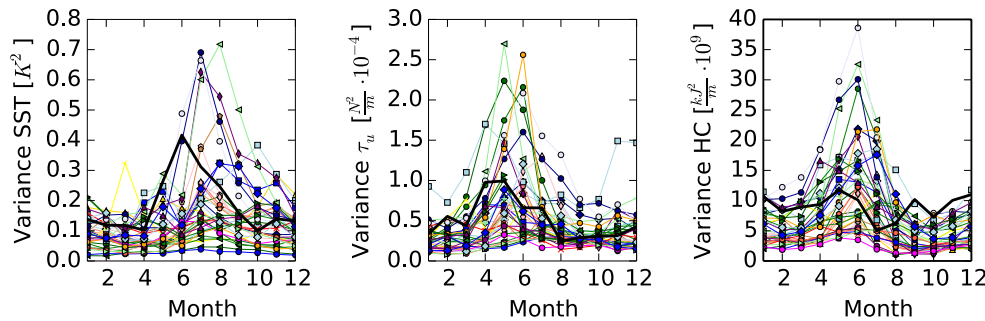


Fig. 7 Seasonal cycles of variance of SST in EA4 [K²], τ_u in WA4 [N²m], and upper ocean HC in EA4 [$\frac{k^2}{m} \cdot 10^9$]. Reanalysis values plotted in black

connected to the missing weakening of τ_u in September as described above.

The oceanic HC displays even larger differences in seasonality with respect to the reanalysis than τ_u and SST. In addition to the large spread between the models, the absolute value of the HC is up to twice as large as that of the ocean reanalysis and there is a distinct lag in annual cycle of the CGCMs with respect to the reanalysis. The seasonal minimum of the HC is clearly misplaced by up to 3 months and the models fail to capture the details of the biannual characteristic. Note that the similarities in the annual cycle of HC shown here and the annual cycle of Z_{20} as shown by Richter [Fig. 6 in Richter and Xie (2008)] demonstrate that HC is a valid measure for the oceanic subsurface condition as indicated by Z_{20} .

In this section, large errors in the annual cycle for each of the three variables that are involved in the BF have been shown, confirming earlier studies, e. g., Richter and Xie (2008), Richter et al. (2014). We continue to show the annual cycle of variances for each of the three variables.

In Fig. 7 shortcomings of the models are distinctly visible. For example, for the variance of τ_u (center panel) we find that the reanalysis data displays a plateau of high variance from April to May, when the winds strengthen. This is also the time when the atmosphere at the equator reacts most strongly to SST' in the east. Most of the models display a single peak which occurs about one to 2 months later in the year than observed. This lagged relationship also appears in the annual cycles of variance for SST and HC. Apart from the lag, there are also large errors in the amplitude of variance in CGCMs compared to the variance in reanalysis. These errors are both positive and negative.

For the reanalysis data, the time frame when the BF is active coincides with the maximum variance of the relevant variables, especially in case of τ_u . SST variance steeply increases in May and peaks in June, when the BF loop is closed. We have found biases in the CGCMs' annual cycles, but does this also imply errors in the simulated BF? This could be expected from the result that the BF is only active

in a particular season in the reanalysis: it needs a specific background state to operate. We investigate this question by correlating the three variable pairs obtained from model output in the same manner as done for the reanalysis, and subsequently compare the spatial response patterns to the pattern obtained from reanalysis by pattern correlation analysis.

4.2 Pattern correlation analysis

To investigate whether a model reproduces the BF we correlate the time series of variable a and b with each other to obtain their coupling pattern as shown for the reanalysis (see Eq. 2). Subsequently, we perform pattern correlation between the model and the reanalysis correlation field, according to Eq. 3. Here, r_{ra} and r_m are the correlation coefficient fields from correlating the variables a and b from the reanalysis and model output, respectively. $\sigma_{r_{ra}} \cdot \sigma_{r_m}$ is the product of the standard deviations of the reanalysis and model correlation fields. Prime denotes anomalies as in Eq. 2.

$$MRA = \frac{\sum r'_{ra}(lat, lon) \cdot r'_m(lat, lon)}{\sigma_{r_{ra}} \cdot \sigma_{r_m}} \quad (3)$$

A model that reproduces the coupling pattern yields a high pattern correlation value. We call this value “model-reanalysis agreement” (MRA), it is plotted on the y-axis of the multi-model comparison plots (Figs. 8, 9). Note that the MRA depends only on the spatial pattern of the response, and not on its correlation strength. Hence much weaker $a - b$ correlation values in the model can still score highly on the MRA axis. To take the correlation between the variable pair into account, we plot the correlation value spatially averaged over the region of interest (i. e., WA4 for $\lambda_{SST \rightarrow \tau_u}$ and EA4 for $\lambda_{\tau_u \rightarrow HC}$ and $\lambda_{HC \rightarrow SST}$) on the x-axis. The original correlation value obtained from the reanalysis is marked as a red line. The ensemble mean correlation strength between the two variables under investigation is marked by a pink line.

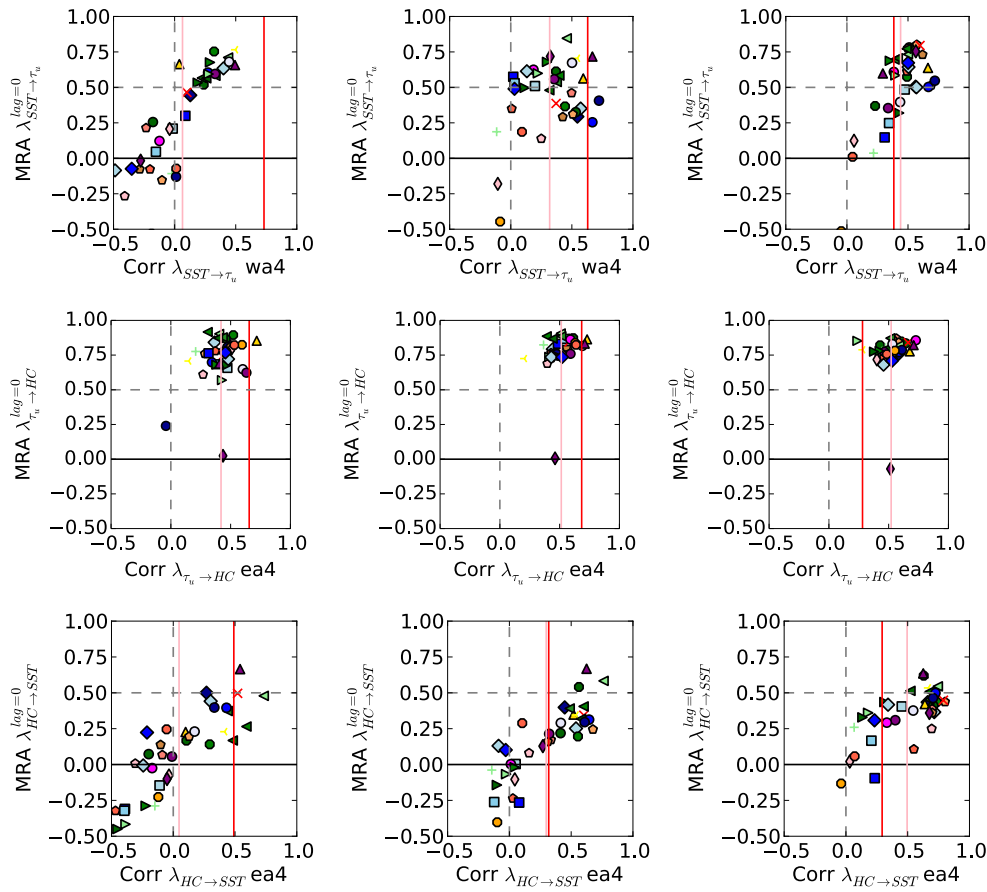


Fig. 8 Pattern correlation between models and reanalysis (MRA) plotted against the correlation value between the two variables of the respective component of the BF averaged over the area of interest. The *red line* denotes the reanalysis correlation value in the region, the

pink line the multi model average. The three columns show the results for May, June and July individually (April on May, May on June, and June on July in the case of $\lambda_{\tau_u \rightarrow HC}$)

For the first component of the feedback, $\lambda_{SST \rightarrow \tau_u}$ (first row), we see an improvement in model performance of $\lambda_{SST \rightarrow \tau_u}$ from May to June (Fig. 8). In May (first row, left panel) the ensemble mean does not simulate the BF, only a few models are located in the upper right of the plot, which means that those CGCMs show some agreement with the reanalysis in both pattern and $\lambda_{SST \rightarrow \tau_u}$ correlation strength. However, none of the models reaches the inter-variable correlation strength obtained from reanalysis. In June (first row, center panel) the overall pattern correlation value increases compared to May, along with an increase in the correlation strength of $\lambda_{SST \rightarrow \tau_u}$. The ensemble mean correlation strength moves closer to the observed one and more models display large pattern agreement with the reanalysis. In July (upper right) the picture is improved again, now most of the models under investigation agree with the reanalysis. Note that in this month the reanalysis pattern of $\lambda_{SST \rightarrow \tau_u}$ does not consist of the pure BF pattern anymore, because the atmospheric response to SST' has moved towards the north.

The second component of the feedback, $\lambda_{\tau_u \rightarrow HC}$, is simulated better by the CGCMs. Throughout the 3 months in boreal summer we investigate, high model–reanalysis agreement (MRA) is obtained. The correlation between τ_u and HC is only slightly underestimated and especially in June nearly all models simulate this component of the feedback loop correctly. In July we observe higher $\tau_u \rightarrow HC$ correlations in the EA4 region than in the reanalysis.

The influence of HC' on overlying SST' at the equator ($\lambda_{HC \rightarrow SST}$) is simulated less accurately. The spatial pattern of this BF component is poorly represented throughout the whole season we investigate. Similarly to $\lambda_{SST \rightarrow \tau_u}$, the MRA scores lowest in May and improves slightly with increasing $\lambda_{HC \rightarrow SST}$ correlation strength in June. Only very few models reach high MRA, even though the correlation strength between HC' and SST' almost reach reanalysis values. As for the other components, the multi-model mean variable correlation strength exceeds the reanalysis value in July, but in this case MRA has not increased significantly. The low MRA shows that, while the CGCMs display an

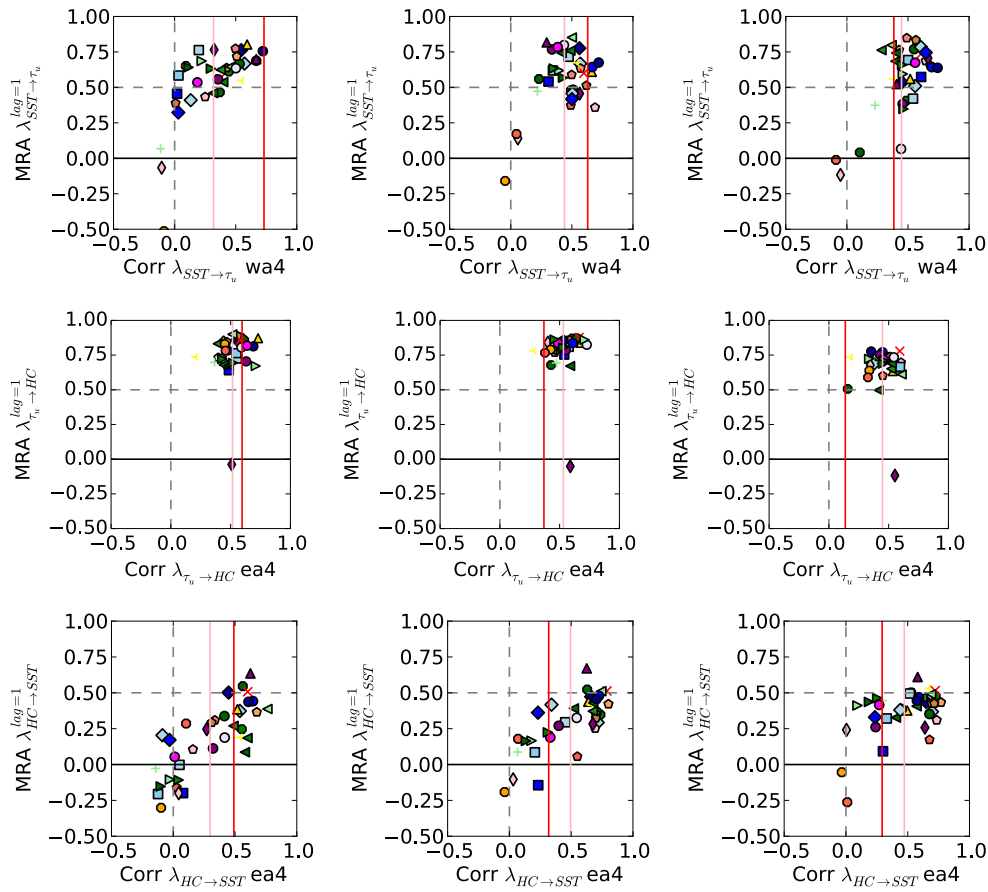


Fig. 9 Pattern correlation vs correlation strength plot, models lagging reanalysis by 1 month. The three columns show the results for May_{reanalysis} compared to June_{model}, June_{reanalysis}—July_{model}, and July_{reanalysis}—August_{model}, respectively

interaction almost as strong as in the reanalysis in the eastern part of the basin, the response pattern is different from the one in the reanalysis. Strong correlations between HC' and SST' are simulated in locations that are absent in the reanalysis and vice versa. This could be due to the fact that we compare basinwide patterns. However, when we restrict the area we use for the pattern correlation to the eastern basin the model–reanalysis agreement is only marginally increased. This indicates that the low MRA also arises from the discrepancy in the spatial representation of $\lambda_{HC \rightarrow SST}$ in the cold tongue region. The same holds for the $HC \rightarrow SST$ correlation strength on the x-axis if we choose a smaller index region (2°N — 2°S , 20°W — 10°E , not shown). Our conclusion is therefore that the third component of the BF is the one represented worst with respect to the spatial structure out of the three components of the BF.

In the following we investigate whether the incorrectly simulated annual cycle is responsible for errors of the simulated BF. Most models display lags of variance by 1–2 months, but the variance does not uniformly lag for all variables. We compare the model correlation patterns to the ones from reanalysis, 1 and 2 months earlier each, that is

May_{Reanalysis} to June_{CGCM}, and so on. Regarding the size of the basin and the time scale on which the BF is active, a longer lag time between reanalysis and CGCM would not be physical. This is determined by the atmospheric and upper ocean adjustment time scales.

By introducing a lag of 1 month, the MRA is drastically improved for $\lambda_{SST \rightarrow \tau_u}$ in all months (cf. Fig. 9). The majority of the models is now situated in the upper right corner of the plot revealing that the pattern response of τ_u' to SST' is similar to the reanalysis response pattern if this lag is taken into account. In August, the CGCMs produce a pattern that is close to the reanalysis pattern in July. This indicates that the atmospheric response move from pure BF to another process, such as following the migration of the ITCZ, as has been suggested earlier.

For $\lambda_{\tau_u \rightarrow HC}$ similar behaviour is observed, even though the agreement between model output and reanalysis is reasonable without a lag as well. This component of the BF is similar to the one in reanalysis in almost all of the models.

The simulation of the third component of the BF, $\lambda_{HC \rightarrow SST}$, is also improved by introducing a lag of 1 month between reanalysis and CGCMs, but here the model output

Fig. 10 Model reanalysis agreement plotted against the absolute error of the upper ocean HC in EA4 for May, June and July. This plot shows that the mean state of the HC does not give indication for the model performance regarding $\lambda_{HC \rightarrow SST}$

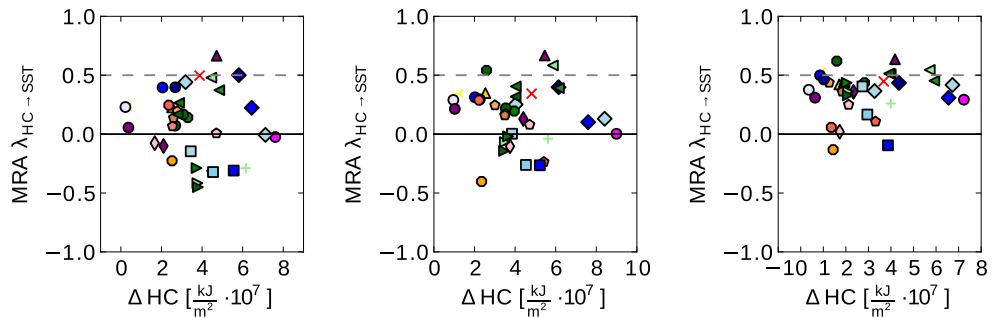
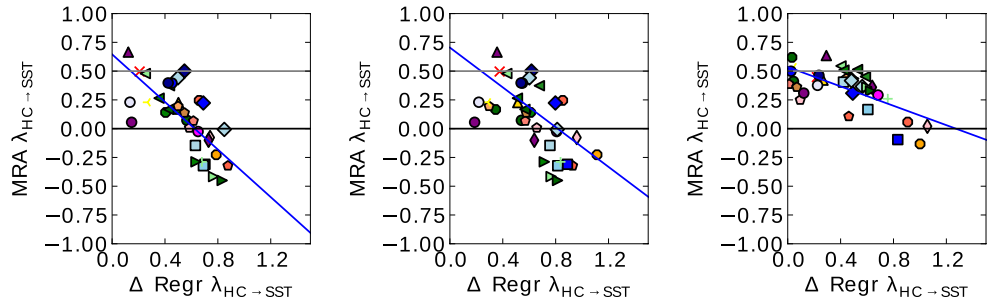


Fig. 11 Pattern correlation plotted against absolute error regression strength for May, June, and July. The bigger the error, the smaller is the model–reanalysis agreement. Hence, the stronger the influence of HC anomaly on SST anomalies, the closer the pattern becomes to a pure BF pattern



does not reach similar agreement with the reanalysis as for $\lambda_{SST \rightarrow \tau_u}$ and $\lambda_{\tau_u \rightarrow HC}$. For all three components of the BF a lag of 2 months yields similar results as a lag of 1 month (not shown).

From the results of this section we conclude that $\lambda_{SST \rightarrow \tau_u}$ and $\lambda_{\tau_u \rightarrow HC}$ of the BF are reasonably well represented by the models, with $\lambda_{\tau_u \rightarrow HC}$ simulated better than $\lambda_{SST \rightarrow \tau_u}$. The pattern of the correlation between HC' and overlying SST', $\lambda_{HC \rightarrow SST}$, is not represented as well. One hypothesis is that the systematic error in the mean state of the thermocline Richter et al. (2014), and hence the HC, is responsible. If this is the case we expect to see a connection between the mean state error of HC in EA4 and the agreement between models and reanalysis $\lambda_{HC \rightarrow SST}$ in such a way that a model which displays a reduced mean state error would score a higher MRA value. However, Fig. 10 reveals that no significant linear connection can be found. The misrepresentation of $\lambda_{HC \rightarrow SST}$ can, hence, not simply be explained by the erroneous mean state (of HC) in the TA basin. Neither is there a connection between the mean state of SST in EA4 and the model performance with respect to simulating $\lambda_{HC \rightarrow SST}$ (not shown). Note that the missing connection might indicate that the CGCMs' mean state is too far removed from the reanalysis to obtain a linear relation.

4.3 Regression values

Linear regression analysis (not shown) reveals that for $\lambda_{SST \rightarrow \tau_u}$ and $\lambda_{\tau_u \rightarrow HC}$, which are reasonably well simulated in the models, there is no consistent connection between

regression strength and MRA. The regression strength is under- and overestimated by the individual models, but without significant connection to the spatial pattern obtained from the correlation analysis. This is consistent with the results of the pattern correlation analysis. However, for $\lambda_{HC \rightarrow SST}$ we notice a relationship between MRA and regression strength. This relationship becomes more obvious when the MRA value is plotted against the absolute error in regression values, as done in Fig. 11. In general, the models underestimate the regression strength of $\lambda_{HC \rightarrow SST}$, especially in May and June. Most models with large absolute errors in regression strength strongly underestimate the actual influence of HC' on SST'. We deduce that a model that shows a larger influence of HC' on overlying SST' is also likely to have a response pattern more similar to the actual response as obtained from reanalysis. In other words, the larger the influence of HC' on SST', the closer the $\lambda_{HC \rightarrow SST}$ pattern is to reanalysis, i. e., the better the BF is simulated.

4.4 Subsurface structure

As we have demonstrated above, the influence of HC' on overlying SST' for the individual models cannot readily be linked to a typical BF pattern in CMIP5 models. In reanalysis, on the other hand, there is a distinct pattern on the equator in May and June. When averaging the response pattern of all models we obtain a pattern (Fig. 12) that is similar to the one obtained from reanalysis (cf. Fig. 5). The correlation strength of $\lambda_{HC \rightarrow SST}$ is, however, much lower than in reanalysis, due to different correlation patterns in

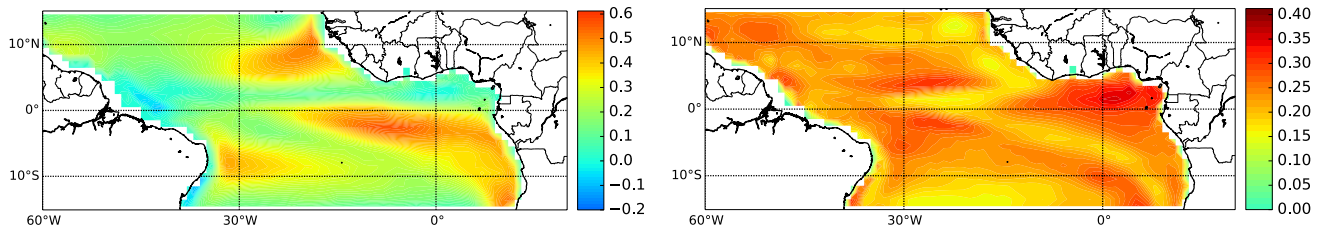


Fig. 12 Left hand side Model ensemble mean response pattern of $\lambda_{HC \rightarrow SST}$. Right hand side standard deviation of correlation values between the individual models for pattern $\lambda_{HC \rightarrow SST}$

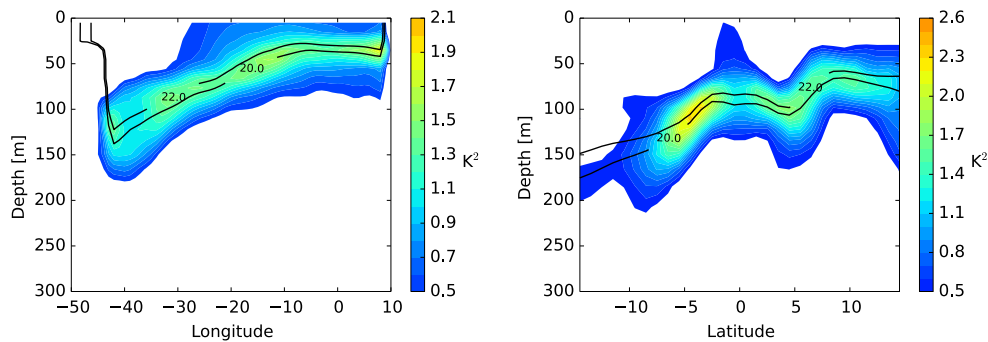


Fig. 13 Equatorial and 30 °W temperature variance cross sections in the month July of the series, upper 300 m of the TA, obtained from reanalysis. Black lines denote the 20 °C and 22 °C isotherms

the different CGCMs. Note that the standard deviation is large all over the basin, which indicates that individual models differ greatly in their representation of $\lambda_{HC \rightarrow SST}$.

We investigate the origin of the inaccurate spatial representation of $\lambda_{HC \rightarrow SST}$ by analysing the subsurface temperatures of the equatorial Atlantic. Two temperature variance cross sections (along the equator and 30°W) are shown for the reanalysis and for each of the models under investigation (Figs. 13, 14, and 15). In regions where the temperature variance extends to the surface, coupling between subsurface (and hence HC) anomalies and SST' is present. In the reanalysis it occurs predominantly at the equator around 10 °W in the EA4 region (Fig. 13). This is vastly misrepresented by the CGCMs. The model output shows large deviations from the reanalysis; coupling from subsurface to surface takes place at different locations, if at all, throughout the months when the BF is active (only July shown). This is also illustrated by the longitude cross section in Fig. 15. Here, off-equatorial temperature anomalies couple with the surface much more than observed in reanalysis.

In the Pacific, Zelle et al. (2004) have identified two mechanisms through which SST' are influenced by HC', the upwelling and the wind coupling pathway. In the former, the subsurface anomaly propagates vertically through mixing and upwelling. In the latter, it propagates along the equatorial thermocline, causes an SST anomaly on the eastern side of the basin (through the upwelling pathway),

which causes a τ_u anomaly over the basin. This τ_u ' influences the SST' overlying the original subsurface anomaly. The wind coupling pathway is considered to be active in the western part of the Pacific, where the thermocline reaches depths of more than 120 m. Where this pathway is active, the thermocline–SST' correlation peaks at lags of 4–8 months. Considering the size of the Atlantic ocean compared to the Pacific, the lag would be considerably shorter if this pathway was active. In the reanalysis the $\lambda_{HC \rightarrow SST}$ correlation peaks at zero month lag, and the thermocline in the eastern part of the Atlantic is very shallow (ca. 50 m). This indicates that the direct pathway is dominant in the eastern part of the TA, where it forms the third component of the BF, $\lambda_{HC \rightarrow SST}$. Some models display growing correlation between HC' and SST' with increasing lag in the western part of the basin, suggesting the presence of the wind coupling pathway (not shown). However, this feature is absent in the reanalysis.

We can obtain more insight into the oceanic origin of the SST' by correlating SST's in the cold tongue region with subsurface temperature anomalies Θ_o' . In the reanalysis a clear picture of the BF and its seasonality is found (Fig. 16). In February and March, SST's in the cold tongue are mostly correlated with SST' in the well mixed surface layer stretched along the equator. In April, when both $\lambda_{SST \rightarrow \tau_u}$ and $\lambda_{\tau_u \rightarrow HC}$ become active, correlation with the underlying ocean temperature Θ_o becomes significant.

Fig. 14 Equatorial temperature variance cross section in the upper 300 m of the TA for each of the models compared in this study, July. *Black lines* as in Fig. 13

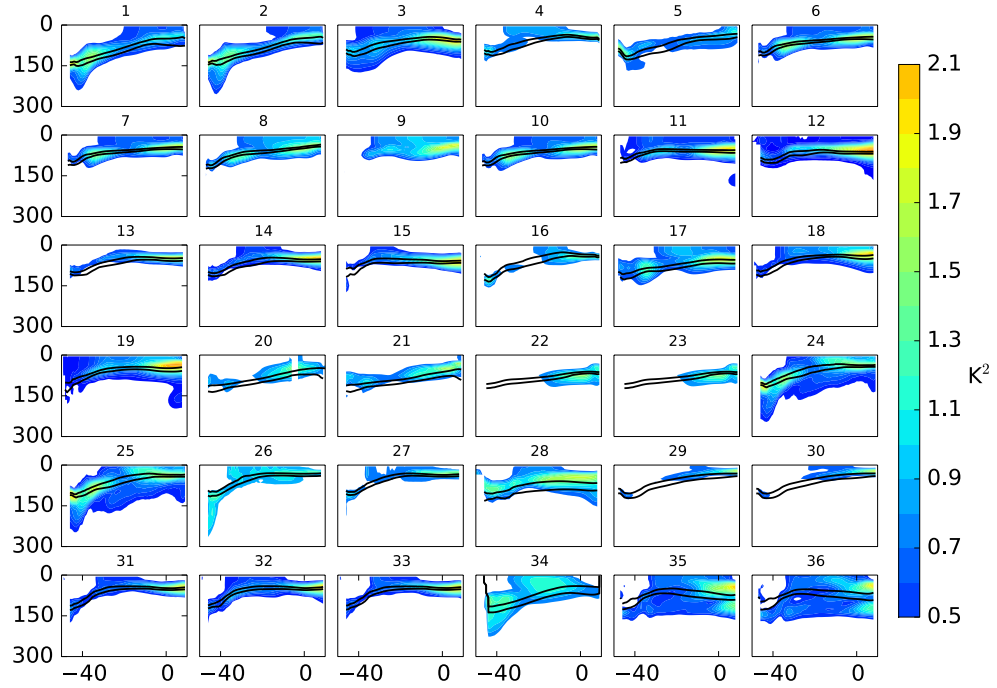
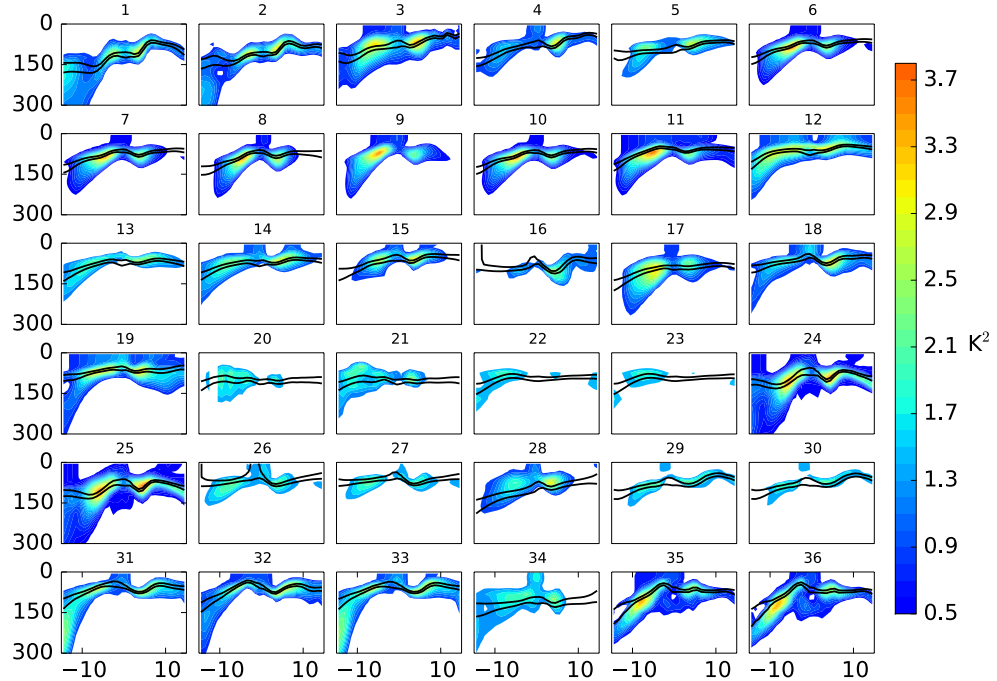


Fig. 15 Temperature variance cross section along 30 °W in the upper 300 m of the TA obtained from model output, July. *Black lines* as in Fig. 13



The coupling strengthens and reaches greater depths in May and June, and retreats in July. In August it has almost disappeared. The correlation between Θ_o' and SST' is significant only in the months when the BF is active. The second Niño in boreal winter can also be seen. It is noteworthy though, that here the correlation between SST_{EA4}' and Θ_o' is more confined to the coast, while in boreal summer it is present in the whole eastern TA. We repeated the previous analysis for each of the individual CGCMs for June

and August. In June (Fig. 17), very few CGCMs display a $SST_{EA4}' - \Theta_o'$ correlation pattern similar to the one in reanalysis. The coupling between subsurface and surface anomalies does not take place adequately. In August (Fig. 18), most models simulate the coupling, although some models display spurious subsurface patterns that are not connected with the surface (e. g. panels five, twelve, and fourteen). These might be associated with meridional current patterns in the CGCMs that are not present in the

Fig. 16 Annual cycle of equatorial $SST_{EA4} - \Theta_o$ correlation, reanalysis data (ORAS4). Contours indicate statistically significant correlation at the 90 % confidence level

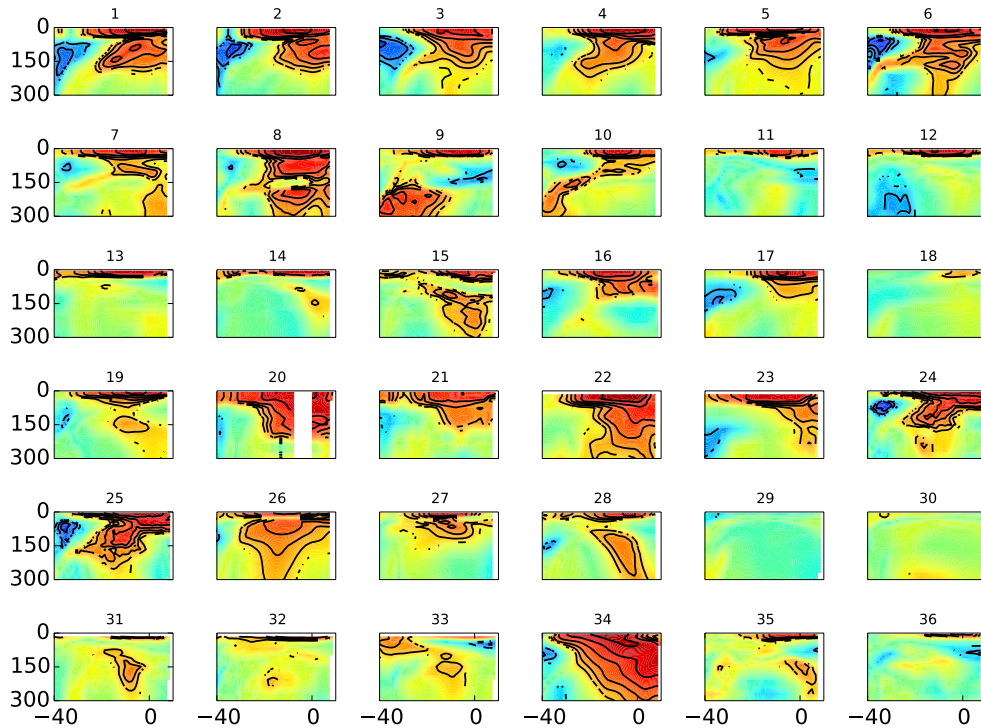
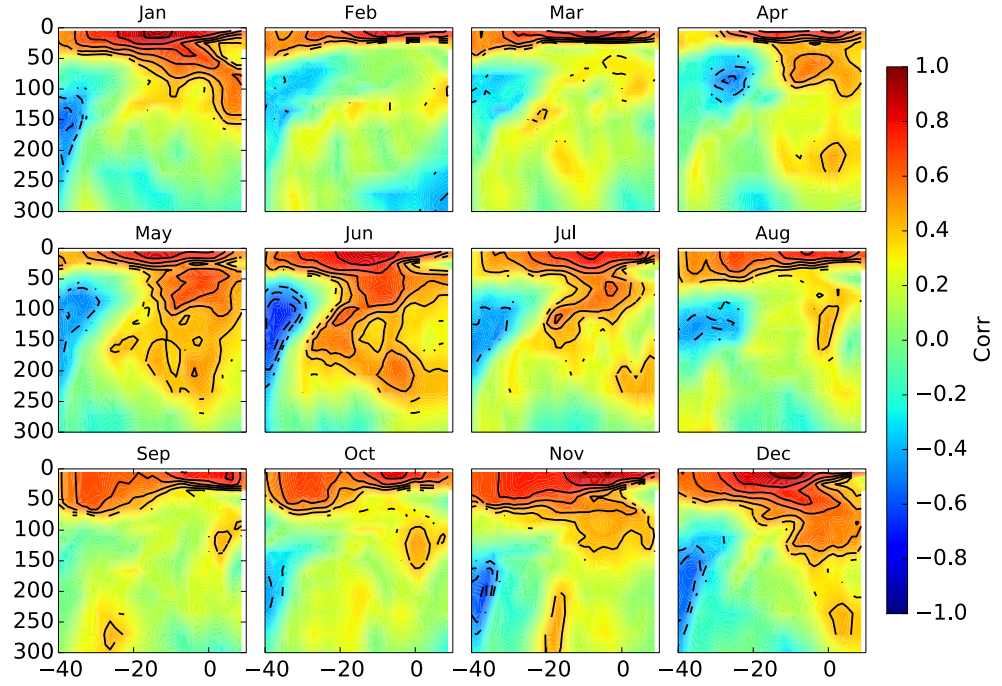


Fig. 17 Model equatorial $SST_{EA4} - \Theta_o$ correlation in June. Contours as Fig. 16. The observed subsurface–surface coupling is simulated by only a few models

reanalysis. Whether this coupling is associated with the BF is questionable. In August the BF loop is no longer closed. The SST_{EA4}' is not centered on the equator anymore, suggesting that other mechanisms, such as the WES feedback, dominate. Note that we compared the correlation

patterns of $\lambda_{SST \rightarrow \tau_u}$ with a lag of 1 month. August in the CGCMs is similar to July in the reanalysis, when the pattern has departed from the equator and the BF coupling is weakening. Some models have already established an $SST_{EA4}' - \Theta_o'$ correlation in July. When that is the case,

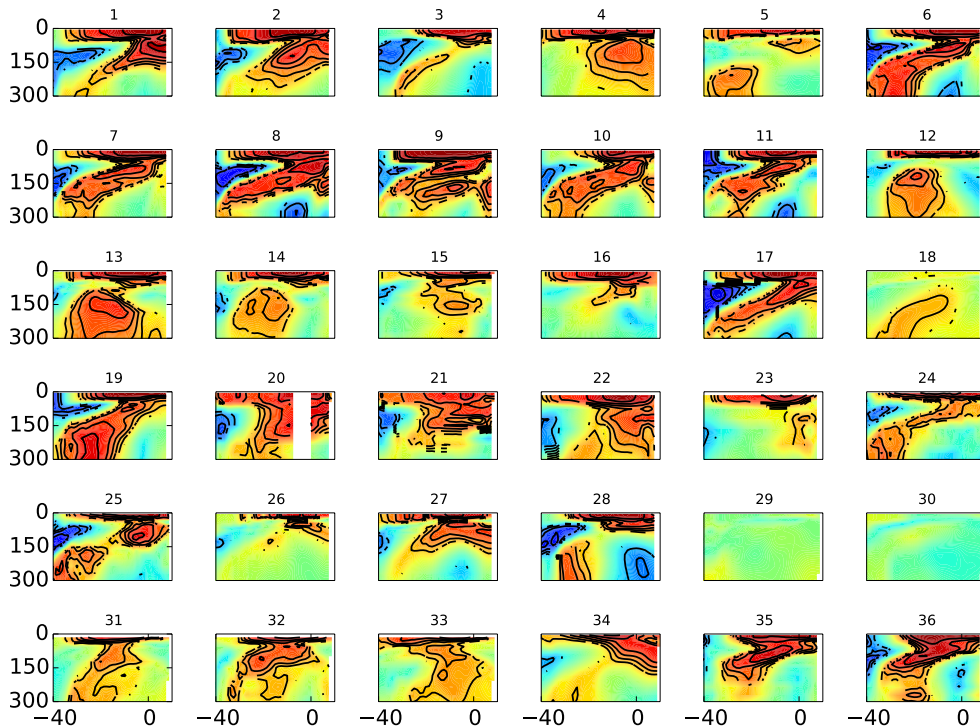


Fig. 18 As Fig. 17, but for August. The CMIP5 models display an interaction between subsurface- and surface temperature later in the year

the models most likely simulate the BF completely. The lack of high MRA values can then be explained by (misrepresented) off-equatorial variability.

5 Conclusion

In this study we investigate the BF in the tropical Atlantic ocean from both reanalysis data and CMIP5 model output. The reanalysis data clearly shows the presence of a zonal mode which is driven by the BF, confirming previous studies. The monthly stratified analysis shows that the BF is not equally active throughout the year, it is strongest in May and June and begins to fade again in July.

$\lambda_{SST \rightarrow \tau_u}$ and $\lambda_{\tau_u \rightarrow HC}$ are reasonably well simulated by the models based on correlation strength and spatial pattern. While τ_u' in the western part of the basin reacts to SST'_{EA4} within a month, we introduce a lag between τ_u' and HC' in order to exclude direct influences of τ_u' on SST' in the eastern part of the basin. By evaluating the eastern equatorial HC' response to $\tau_u'_{WA4}$ with a lag of 1 month we allow for a Kelvin wave to propagate from west to east.

The agreement of $\lambda_{SST \rightarrow \tau_u}$ and $\lambda_{\tau_u \rightarrow HC}$ between reanalysis and model output improves further when introducing a lag of 1 month between them, correcting for the lag of the annual cycle (of variance) in the CGCMs. We conclude that the physical mechanisms behind $\lambda_{SST \rightarrow \tau_u}$ and $\lambda_{\tau_u \rightarrow HC}$ are

simulated well by the models, but that the lag in the annual cycle introduces a lag in the timing of the BF.

$\lambda_{HC \rightarrow SST}$, on the other hand, is generally not well represented by the models. The patterns of the responses of CGCM output and reanalysis agree to less than 25 % in almost all cases. We note that there is a significant correlation between HC' and SST' in the eastern part of the basin, but its location and pattern are significantly different from the one detected in reanalysis. No significant linear correlation between mean state error of the HC in the eastern part of the basin and the model–reanalysis agreement could be found, so the reason for the error in the third component of the loop could not conclusively be linked to the mean state bias of SST and HC . This does not exclude the possibility that individual models perform better when their mean state is corrected. In fact, this was recently shown to be the case for the Kiel Climate Model, which does not belong to the CGCM ensemble investigated here (Ding et al. 2015). We speculate that differences between the mean state of the CGCMs and the reanalysis mean state may be too large to display a linear relationship between the mean state error and the performance with respect to the BF.

Examining the subsurface temperature variance provides insight into the origin of the largely varying $\lambda_{HC \rightarrow SST}$ response fields. This component of the BF describes an interaction between subsurface and surface anomalies. In the equatorial cross section of temperature variance in the

reanalysis there is a clear connection between subsurface and surface anomalies. Here, mixing takes place and SST is influenced by subsurface temperatures. None of the models is able to reproduce this structure. Hence, while there is some interaction indicated by the $\lambda_{HC \rightarrow SST}$ correlation, the location of this interaction is different from reanalysis. This is also demonstrated by longitude–depth cross sections that show $SST_{EA4'} - \Theta_o'$ correlations. The seasonality displayed by reanalysis is modelled by hardly any of the CGCMs. When the correlation decreases in reanalysis, it increases in the models and even persists throughout the year (not shown).

The timing between $\lambda_{SST \rightarrow \tau_u}$ and $\lambda_{\tau_u \rightarrow HC}$ and the subsurface–surface coupling is misplaced in such a way that the full BF loop is most likely not closed for most of the models. $\lambda_{HC \rightarrow SST}$ in the CGCMs becomes active too late in the year. The center of atmospheric sensitivity to $SST_{EA4'}$ has moved north of the equator, indicating that other processes play a more important role than the BF along the equator. The lack of seasonality displayed in $SST_{EA4'} - \Theta_o'$ in the CGCMs hints on other processes inducing the $SST_{EA4'} - \Theta_o'$ coupling, rather than being initiated by the BF.

Based on the results of this study, we conclude that the erroneous vertical oceanic stratification influences the interannual variability in the region by hindering $\lambda_{HC \rightarrow SST}$ from being represented correctly.

Even though the models display an SST annual cycle much weaker than in reanalysis, $\lambda_{SST \rightarrow \tau_u}$ and $\lambda_{\tau_u \rightarrow HC}$ are reasonably well simulated, albeit with an error in timing because of the lags in seasonality. This disproves our hypothesis that the functioning of the BF depends on the correctly simulated annual cycle. The mean state of the TA is misrepresented in the CGCMs, but the influence of perturbations of variable a (SST, τ_u) on variable b (τ_u , HC) is still present. This is in line with earlier findings that even though the mean state of the TA is heavily biased, interannual variability can still be reasonably represented Richter et al. (2014). However, biases in the subsurface temperature variance affect the spatial pattern of $\lambda_{HC \rightarrow SST}$. $\lambda_{HC \rightarrow SST}$ explains a large part of SST variability in the region, and exactly this part of the feedback is not simulated well.

The errors in the simulated subsurface thermal structure can be due to both ocean mixing and/or arise from shortcomings of the atmospheric forcing which sets the structure of the ventilated thermocline. This should be the focus of further investigation and a starting point for work on model improvement in order to improve the HC–SST relationship in the eastern tropical Atlantic.

Acknowledgments We thank the anonymous reviewers for their helpful comments and suggestions. The authors would also like to thank Noel Keenlyside for helpful discussion and constructive comments, and Folmer Krikken for reading and improving this work. The research leading to these results received funding from the

EU FP7/2007-2013 under Grant Agreement No. 603521, project PREFACE.

Open Access This article is distributed under the terms of the Creative Commons Attribution 4.0 International License (<http://creativecommons.org/licenses/by/4.0/>), which permits unrestricted use, distribution, and reproduction in any medium, provided you give appropriate credit to the original author(s) and the source, provide a link to the Creative Commons license, and indicate if changes were made.

References

- Balmaseda MA, Mogensen K, Weaver AT (2013) Evaluation of the ECMWF ocean reanalysis system ORAS4. *Q J R Meteor Soc* 139(674):1132–1161. doi:[10.1002/qj.2063](https://doi.org/10.1002/qj.2063)
- Breugem WP, Hazeleger W, Haarsma R (2006) Multimodel study of tropical Atlantic variability and change. *Geophys Res Lett.* doi:[10.1029/2006GL027831](https://doi.org/10.1029/2006GL027831)
- Burls N, Reason C, Penven P, Philander S (2011) Similarities between the tropical Atlantic seasonal cycle and ENSO: an energetics perspective. *J Geophys Res Oceans.* doi:[10.1029/2011JC007164](https://doi.org/10.1029/2011JC007164)
- Burls N, Reason C, Penven P, Philander S (2012) Energetics of the tropical Atlantic zonal mode. *J Clim.* doi:[10.1175/JCLI-D-11-00602.1](https://doi.org/10.1175/JCLI-D-11-00602.1)
- Carton JA, Cao X, Giese BS, Da Silva AM (1996) Decadal and interannual SST variability in the tropical Atlantic Ocean. *J Phys Oceanogr.* doi:[10.1175/1520-0485\(1996\)026<1165:DAISVI>2.0.CO;2](https://doi.org/10.1175/1520-0485(1996)026<1165:DAISVI>2.0.CO;2)
- Chang CY, Carton JA, Grodsky SA, Nigam S (2007) Seasonal climate of the tropical Atlantic sector in the NCAR community climate system model 3: error structure and probable causes of errors. *J Clim* 20(6):1053–1070. doi:[10.1175/JCLI4047.1](https://doi.org/10.1175/JCLI4047.1)
- Chang P, Ji L, Li H (1997) A decadal climate variation in the tropical Atlantic Ocean from thermodynamic air–sea interactions. *Nature* 385(6616):516–518. doi:[10.1038/385516a0](https://doi.org/10.1038/385516a0)
- CMIP5 (2015) Coupled Model Intercomparison Project, W.C.R.P. <http://cmip-pcmdi.llnl.gov/cmip5/availability.html>. Accessed 16 July 2015
- Davey M, Huddleston M, Sperber K, Braconnot P, Bryan F, Chen D, Colman R, Cooper C, Cubasch U, Delecluse P et al (2002) STOIC: a study of coupled model climatology and variability in tropical ocean regions. *Clim Dynam* 18(5):403–420. doi:[10.1007/s00382-001-0188-6](https://doi.org/10.1007/s00382-001-0188-6)
- Dee D, Uppala S, Simmons A, Berrisford P, Poli P, Kobayashi S, Andrae U, Balmaseda M, Balsamo G, Bauer P et al (2011) The ERA-interim reanalysis: configuration and performance of the data assimilation system. *Q J R Meteor Soc* 137(656):553–597. doi:[10.1002/qj.828](https://doi.org/10.1002/qj.828)
- DeWitt DG (2005) Diagnosis of the tropical Atlantic near-equatorial SST bias in a directly coupled atmosphere-ocean general circulation model. *Geophys Res Lett.* doi:[10.1029/2004GL021707](https://doi.org/10.1029/2004GL021707)
- Ding H, Keenlyside N, Latif M (2009) Seasonal cycle in the upper equatorial Atlantic Ocean. *J Geophys Res.* doi:[10.1029/2009JC005418](https://doi.org/10.1029/2009JC005418)
- Ding H, Keenlyside N, Latif M (2010) Equatorial Atlantic interannual variability: role of heat content. *J Geophys Res.* doi:[10.1029/2010JC006304](https://doi.org/10.1029/2010JC006304)
- Ding H, Keenlyside N, Latif M, Park W, Wahl S (2015) The impact of mean state errors on equatorial Atlantic interannual variability in a climate model. *J Geophys Res Oceans.* doi:[10.1002/2014JC010384](https://doi.org/10.1002/2014JC010384)
- Foltz GR, McPhaden MJ (2010) Interaction between the Atlantic meridional and Niño modes. *Geophys Res Lett.* doi:[10.1029/2010GL044001](https://doi.org/10.1029/2010GL044001)

- Hazeleger W, Haarsma RJ (2005) Sensitivity of tropical Atlantic climate to mixing in a coupled ocean-atmosphere model. *Clim Dynam* 25(4):387–399. doi:[10.1007/s00382-005-0047-y](https://doi.org/10.1007/s00382-005-0047-y)
- Janssen MF, Dommegård D, Keenlyside N (2008) Tropical atmosphere–Ocean interaction in a conceptual framework. *J Clim.* doi:[10.1175/2008JCLI2243.1](https://doi.org/10.1175/2008JCLI2243.1)
- Keenlyside NS, Latif M (2007) Understanding equatorial Atlantic interannual variability. *J Clim* 20:131–142. doi:[10.1175/JCLI3992.1](https://doi.org/10.1175/JCLI3992.1)
- Laboratory NP (2015) Website http://www.kayelaby.npl.co.uk/general_physics/2_7/2_7_9.html. Accessed 23 Feb 2015
- Li G, Xie SP (2012) Origins of tropical-wide SST biases in CMIP multi-model ensembles. *Geophys Res Lett.* doi:[10.1029/2012GL053777](https://doi.org/10.1029/2012GL053777)
- Lübecke JF, Böning CW, Keenlyside NS, Xie S (2010) On the connection between Benguela and equatorial Atlantic Niño and the role of the South Atlantic Anticyclone. *Geophys Res Lett.* doi:[10.1029/2009JC005964](https://doi.org/10.1029/2009JC005964)
- Mahajan S, Saravanan R, Chang P (2009) The role of the wind-evaporation-sea surface temperature (WES) feedback in air-sea coupled tropical variability. *Atmos Res* 94(1):19–36. doi:[10.1016/j.atmosres.2008.09.017](https://doi.org/10.1016/j.atmosres.2008.09.017)
- Mitchell TP, Wallace JM (1992) The annual cycle in equatorial convection and sea surface temperature. *J Clim.* doi:[10.1175/1520-0442\(1992\)005<1140:TACIEC>2.0.CO;2](https://doi.org/10.1175/1520-0442(1992)005<1140:TACIEC>2.0.CO;2)
- Muñoz E, Weijer W, Grodsky SA, Bates SC, Wainer I (2012) Mean and variability of the tropical Atlantic Ocean in the CCSM4. *J Clim* 25(14):4860–4882. doi:[10.1175/JCLI-D-11-00294.1](https://doi.org/10.1175/JCLI-D-11-00294.1)
- Okumura Y, Xie SP (2006) Some overlooked features of tropical Atlantic climate leading to a new Niño-like phenomenon. *J Clim* 19(22):5859–5874. doi:[10.1175/JCLI3928.1](https://doi.org/10.1175/JCLI3928.1)
- Richter I, Xie SP (2008) On the origin of equatorial Atlantic biases in coupled general circulation models. *Clim Dynam* 31(5):587–598. doi:[10.1007/s00382-008-0364-z](https://doi.org/10.1007/s00382-008-0364-z)
- Richter I, Xie SP, Behera S, Doi T, Masumoto Y (2014) Equatorial Atlantic variability and its relation to mean state biases in CMIP5. *Clim Dynam* 42(1–2):171–188. doi:[10.1007/s00382-012-1624-5](https://doi.org/10.1007/s00382-012-1624-5)
- Ruiz-Barradas A, Carton JA, Nigam S (2000) Structure of interannual-to-decadal climate variability in the tropical Atlantic sector. *Am Met Soc.* doi:[10.1175/1520-0442\(2000\)013<3285:SOITDC>2.0.CO;2](https://doi.org/10.1175/1520-0442(2000)013<3285:SOITDC>2.0.CO;2)
- Taylor KE, Stouffer RJ, Meehl GA (2012) An overview of CMIP5 and the experiment design. *B Am Meteorol Soc.* doi:[10.1175/BAMS-D-11-00094.1](https://doi.org/10.1175/BAMS-D-11-00094.1)
- Xie SP, Carton JA (2004) Tropical Atlantic variability: patterns, mechanisms, and impacts. *Earth climate: the Ocean–atmosphere interaction. Geophys Monogr* 147:121–142
- Zebiak SE (1993) Air-sea interaction in the equatorial Atlantic region. *J Clim.* doi:[10.1175/1520-0442\(1993\)006<1567:AIITEA>2.0.CO;2](https://doi.org/10.1175/1520-0442(1993)006<1567:AIITEA>2.0.CO;2)
- Zelle H, Appeldoorn G, Burgers G, Oldenborgh GJV (2004) The relationship between sea surface temperature and thermocline depth in the Eastern equatorial Pacific. *Am Met Soc.* doi:[10.1175/2523.1](https://doi.org/10.1175/2523.1)